Combined Rotation Profile and Plasma Stored Energy Control for the DIII-D Tokamak via MPC

William Wehner, Justin Barton, and Eugenio Schuster

***Abstract*— Tokamak plasma rotation is widely recognized for its importance to heat confinement and plasma stability. In this work we consider control of the plasma rotation profile with the aim of building a control strategy suitable for testing various rotation profiles for stability characteristics and reaching desired operating conditions. To obtain a control-oriented model of the toroidal rotation profile evolution, a simplified version of the momentum balance equation is combined with scenario-specific models for the momentum sources. Various momentum sources including on-axis and off-axis neutral beam injection and the non-axisymmetric field coils, which provide rotation damping, allow not only control of the bulk plasma rotation, but also control of the profile shape. A feedback controller is designed in a model predictive control framework to regulate the rotation profile while satisfying constraints associated with the desired plasma stored energy and β (kinetic to magnetic pressure ratio) limits.**

I. Introduction

In the tokamak, an experimental fusion-energy-production device, a plasma (hot ionized gas), typically of hydrogen ions, is confined by magnetic fields and heated to temperatures on the order of 100s of millions of degrees. At such high temperatures, collisions between ions can overcome the repulsive forces due to their Coulomb fields resulting in fusion reactions. The tokamak uses magnetic fields to shape the plasma into a torus (donut) shape as shown in Fig. 1. Individual charged particles are bound to the field lines by the Lorentz Force but are free to travel along the field lines.

The net sum of individual particle velocities along the field lines constitutes the bulk plasma rotation around the torus, denoted Ω_ϕ (angular frequency). It is generally accepted that plasma rotation can contribute to both stability and confinement in tokamak plasmas. The confinement in a tokamak is governed by the radial transport of energy from the plasma center to the plasma edge. A large part of this transport is driven by turbulence. Toroidal rotation, or its shear (profile gradient), has also been recognized as a stabilizing mechanism for deleterious magnetohydrodynamic (MHD) instabilities such as the neoclassical tearing mode (NTM) [1] and the resistive wall mode (RWM) [2]. If not suppressed, such MHD instabilities would otherwise limit the achievable β, ratio of plasma pressure to confining magnetic field pressure. The β represents a measure of efficiency of confinement since it defines how much magnetic confining pressure is required to maintain a particular plasma kinetic pressure. Naturally, the higher β that can be achieved under stable conditions, the better. Higher β implies a higher percentage of fusion reactions for a given magnetic field strength, an important consideration for a commercial device.

Neutral beam injection (NBI) is the dominant source of momentum (and therefore rotation) in present-day tokamaks [3]. NBI consists of injecting beams of highly energetic neutral particles into the plasma, heating the plasma through collisions, and transferring momentum. NBI also enables a technique known as charge exchange spectroscopy [4], which is used to measure the rotation across the plasma radius. This work considers in particular the DIII-D tokamak, located in San Diego, California, USA, which has eight NBI sources with varying configurations relative to the plasma.

Ambient or purposefully imposed non-axisymmetric magnetic fields (NRMF) (perturbations from the perfectly symmetric tokamak field configuration) create a drag force on the plasma rotation, an effect known as neoclassical toroidal viscosity (NTV) [5]. Recent experiments have observed that static NRMF fields tend to drag the rotation to a negative offset [6], allowing spin-up of rotation in the counter-current direction. Plasma acceleration has also been achieved using rapidly rotating resonant fields [7], creating a "forward drag".

In addition to the NBI and NRMF torque sources, six radio-frequency (RF) wave generators are available to inject energy into the plasma. The RF waves resonate with the gyro-kinetic orbit of the electrons, heating the plasma by an effect known as electron cyclotron resonant heating (ECRH).

Recent works have considered rotation profile control for DIII-D [8] and NSTX (spherical torus) [9] using linear model-based controllers that consider actuator constraints passively by the use of an anti-windup compensator. The model-predictive control (MPC) framework considered in this work naturally allows the explicit incorporation of actuator constraints into the design, and also provides the capability to avoid operation limits associated with high β. This work is organized as follows. The model structure is briefly described in Section II. The model-based control design for simultaneous regulation of the rotation profile and plasma stored energy evolution via MPC is considered in Section III. The effectiveness of the controller is examined in Section IV via a simulation study with comparison to the unconstrained, linear-quadratic-regulator approach of previous work [8]. Finally, conclusions are made in Section V.

This work was supported in part by the U.S. Department of Energy (DE-SC0010661). W. Wehner (wehner@lehigh.edu), J. Barton, and E. Schuster are with the Department of Mechanical Engineering and Mechanics, Lehigh University, Bethlehem, PA 18015, USA. We would like to extend special thanks to Jeremy Hanson (General Atomics) and Imene Goumiri (Princeton Plasma Physics Laboratory) for valuable discussion, suggestions, and insight.

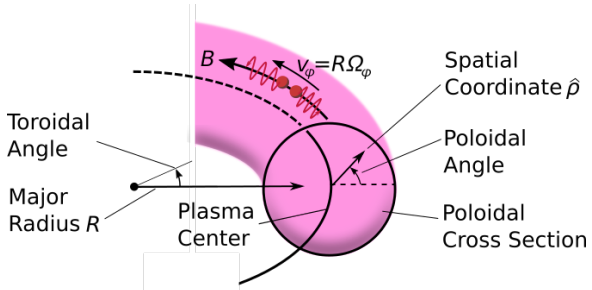

Fig. 1. The tokamak uses magnetic fields to confine a plasma in the shape of a torus. The net sum of individual particle flows along the field lines constitutes the plasma rotation, Ω_ϕ.

II. Modeling the Toroidal Angular Rotation and Plasma Stored Energy

In this work we are interested in the spatial and temporal evolution of the toroidal angular rotation profile and the temporal evolution of the plasma stored energy in response to the various actuators (NBI, ECRH, NRMF). A complete treatment of the the parabolic partial differential equation that describes the toroidal angular momentum (mass density times angular rotation) can be found in [10], [11]. With certain simplifying assumptions [8], we can obtain an approximate diffusive model which captures the dominant dynamics,

$$\begin{aligned} n_{\mathrm{i}} m_{\mathrm{i}} \langle R^2 \rangle \frac{\partial \Omega_\phi}{\partial t} + m_{\mathrm{i}} \langle R^2 \rangle \Omega_\phi \frac{\partial n_{\mathrm{i}}}{\partial t} &= \eta_{\mathrm{NBI}} + \eta_{\mathrm{NRMF}} \\ + \frac{1}{\hat{\rho}\hat{H}} \frac{\partial}{\partial \hat{\rho}} \left[\hat{\rho} \hat{H} n_{\mathrm{i}} m_{\mathrm{i}} \chi_\phi \langle R^2 \left(\nabla \hat{\rho}\right)^2 \rangle \frac{\partial \Omega_\phi}{\partial \hat{\rho}} \right]. \end{aligned} \tag{1}$$

The spatial coordinate ρ, depicted in Fig. 1, can be expressed in terms of the toroidal magnetic flux, Φ, and the toroidal field strength at the plasma center, $B_{\phi,0}$, i.e. $\pi B_{\phi,0} \rho^2 = \Phi$. Normalized ρ, denoted by $\hat{\rho}$, is defined as ρ/ρ_{b}, where ρ_{b} is the value of ρ at the last closed magnetic flux surface. Plasma rotation is denoted by Ω_ϕ, the parameters m_{i} and n_{i}, are the single fluid ion mass and ion density, χ_ϕ is the effective angular momentum diffusivity coefficient (assuming the transport is purely diffusive), $\eta_{(\cdot)}$ represents the local torque density from NBI and NRMF sources, the operator $\langle \cdot \rangle$ stands for flux surface average, R is the major radius of the plasma (see Fig. 1), and $\hat{H}$ is a spatial geometric factor specific to the magnetic configuration in the DIII-D tokamak. The parameters R and $\hat{H}$ are functions of the spatial coordinate $\hat{\rho}$, which depend on the specific geometry and operating regime of the tokamak. These parameters are determined with the analysis code TRANSP for the particular regime of interest [8], [12].

The plasma stored energy, i.e. volume averaged energy density over the plasma volume, can be well approximated by the nonlinear first order system,

$$\frac{dE}{dt} = -\frac{E}{\tau_{\mathrm{E}}} + P_{\mathrm{tot}}(t), \tag{2}$$

where τ_{E} is the global energy confinement time. We use the ITER-98 (IPB98$(y,2)$) [13] scaling law to model the energy confinement time, $\tau_E \propto I_p^{0.93} \bar{n}_e^{0.41} P_{\mathrm{tot}}^{-0.69}$. The total absorbed power, P_{tot} is equal to the auxiliary power injected into the plasma by NBI and ECRH, $P_{\mathrm{aux}} = \sum_{\xi=1}^{n_{\mathrm{NBI}}} P_{\mathrm{NBI},\xi} + P_{\mathrm{EC}}$, plus ohmically driven power from coils, P_{ohm}, minus the radiative power, P_{rad}, i.e. $P_{\mathrm{tot}} = P_{\mathrm{aux}} + P_{\mathrm{ohm}} - P_{\mathrm{rad}}$. The ohmic heating power is a function of the poloidal magnetic flux, therefore a complete model must also consider the poloidal flux evolution. A control-oriented model of the poloidal flux evolution combining the magnetic diffusion equation with physics-based correlations for the electron temperature, plasma resistivity, and non-inductive current drive sources has already been developed for DIII-D [12]. We can write

$$\frac{\partial \psi}{\partial t} = \eta(T_e) k_1 \frac{\partial}{\partial \hat{\rho}} \left(k_2 \frac{\partial \psi}{\partial \hat{\rho}} \right) + k_3 \eta(T_e) j_{\mathrm{ni}}, \tag{3}$$

where the parameters k_1, k_2, and k_3 are time-constant spatial profiles associated with the particular plasma shape and regime of interest, $j_{\mathrm{ni}}(\hat{\rho}, t)$ represents the sum total of non-inductive current drive sources, and $\eta(T_e(\hat{\rho}, t))$ is the resistivity which is dependent on the electron temperature profile, $T_e(\hat{\rho}, t)$, and $\psi(\hat{\rho}, t)$ is the poloidal magnetic flux profile. The toroidal current density profile, $j_{\mathrm{tor}}(\hat{\rho}, t)$ can be expressed as a function of the poloidal flux, and integrating over the plasma volume we can compute the total ohmic power,

$$j_{\mathrm{tor}} = -c_1 \frac{\partial}{\partial \hat{\rho}} \left(c_2 \frac{\partial \psi}{\partial \hat{\rho}} \right), \quad P_{\mathrm{ohm}} = \int_V j_{\mathrm{tor}}^2 \eta(T_e) dV, \tag{4}$$

where c_1 and c_2 are time-constant profiles [12]. The radiative power (Bremsstrahlung radiation) can be expressed as

$$P_{\mathrm{rad}} = \int_V k_{\mathrm{brem}} Z_{\mathrm{eff}} n_e(\hat{\rho}, t)^2 \sqrt{T_e(\hat{\rho}, t)} dV, \tag{5}$$

where $k_{\mathrm{brem}} = 5.5 \times 10^{-37}$ $\mathrm{Wm}^3/\sqrt{keV}$ is the Bremsstrahlung radiation coefficient and Z_{eff} is the effective ion charge [14], and $n_e(\hat{\rho}, t)$ is the electron density profile.

To simulate the system, we must combine equations (1)-(5) with suitable boundary conditions. For the momentum diffusion equation, the boundary conditions are determined from symmetry at the plasma center and an assumed no slip condition at the plasma edge,

$$\frac{\partial \Omega_\phi}{\partial \hat{\rho}}(0, t) = 0, \qquad \Omega_\phi(1, t) = 0, \tag{6}$$

and for the poloidal flux diffusion, they are given by

$$\frac{\partial \psi}{\partial \hat{\rho}}(0, t) = 0, \quad \frac{\partial \psi}{\partial \hat{\rho}}(1, t) = -k_{I_p} I_{\mathrm{p}}(t), \tag{7}$$

where k_{I_p} is a constant and I_p is the total plasma current. Scenario-specific empirical models of the density and temperature profiles [12], and torque sources [8] are combined with (1) and (3) to obtain a control-oriented model of the toroidal rotation profile evolution.

III. Control System Design

In this section, a constrained, predictive feedback controller based on the first-principles-driven model (1)-(7) is proposed for the simultaneous regulation of the toroidal angular rotation profile and plasma stored energy.

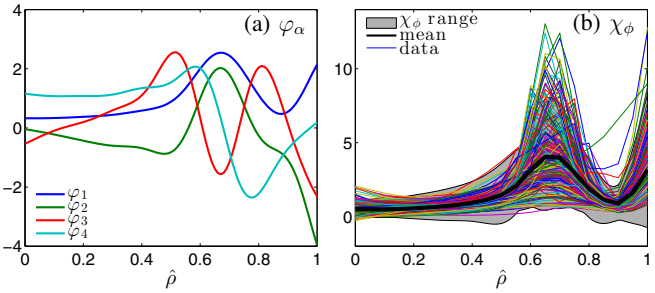

Fig. 2. (a.) POD modes that serve as a basis for χ_ϕ. (b.) The time average of χ_ϕ (black line) based on DIII-D shot 147634 over the time period $t = 2-5$ s, i.e. the current flattop phase. The lines show snapshots of χ_ϕ during the current flattop phase and grey area shows the range covered by the uncertainty model.

A. Discretization by Finite Element Method

The infinite-dimensional model (1) in $\hat{\rho}$ is transformed into a finite dimensional model using the finite-element method. First, the rotation and diffusivity terms are approximated by

$$\Omega_\phi(\hat{\rho},t) \approx \sum_{k=1}^{l_\omega} \omega_k(t)\phi_k(\hat{\rho}), \quad \chi_\phi(\hat{\rho}) \approx \sum_{\alpha=1}^{l_\chi} \gamma_\alpha \varphi_\alpha(\hat{\rho}), \tag{8}$$

where the basis $\{\phi_k \mid k = 1,2,\ldots,l_\omega\}$, is chosen as a set of cubic splines on a finite support that satisfy the boundary conditions (6). The basis $\{\varphi_\alpha \mid \alpha = 1,2,\ldots,l_\chi\}$ is obtained by the proper orthogonal decomposition (POD) method described in [15]. The POD modes $\{\varphi_\alpha \mid \alpha = 1,2,\ldots,l_\chi\}$ obtained for χ_ϕ based on DIII-D shot 147634 are shown in Fig. 2(a), as well as the expected range modeled as a linear combination of the modes in Fig. 2(b). The method of POD modes has the advantage of obtaining a basis with relatively low dimension compared to using splines.

The anomalous variability of χ_ϕ is incorporated in the POD coefficients $(\gamma_1,\gamma_2,\ldots,\gamma_{l_\chi})$, which are modeled in this work as uncertain parameters. To include the uncertainty explicitly, we can write each γ_α as a nominal term plus an additive uncertainty $\gamma_\alpha^0 + \gamma_\alpha^1\delta_\alpha$, $|\delta_\alpha| \le 1$ for all α. Varying each of the δ_α, the value of χ_ϕ varies within the range represented by the grey area of Fig. 2(b).

Combining (1) and (8), as described in [8] yields a nonlinear, finite dimensional, uncertain model,

$$\dot{\boldsymbol{\omega}} = \boldsymbol{F}(\boldsymbol{\omega},\boldsymbol{u},\boldsymbol{\delta}) \tag{9}$$

where $\boldsymbol{\omega} = (\omega_1,\omega_2,\ldots,\omega_{l_\omega})$, $\boldsymbol{u} = (\dot{\bar{n}}_\mathrm{i}, \bar{n}_\mathrm{i}, P_\mathrm{EC}, P_{\mathrm{NB},1},\ldots,P_{\mathrm{NB},n_\mathrm{NB}}, I_\mathrm{NRMF})$, and $\boldsymbol{\delta} = (\delta_1,\ldots,\delta_{l_\chi})$.

B. Model Linearization

The plasma density is difficult to control in tokamaks because of weak actuation, therefore deviations of the density from the desired operating point will be treated as an input disturbance. Moreover, the first two NBI are dedicated to diagnostics. To account for this we split the input $\boldsymbol{u}$ into the controlled input $\boldsymbol{u}^\mathrm{c} = (P_\mathrm{EC}, P_{\mathrm{NBI},3},\ldots,P_{\mathrm{NBI},n_\mathrm{NBI}}, I_\mathrm{NRMF})$ and the uncontrolled input $\boldsymbol{u}^\mathrm{nc} = (P_{\mathrm{NBI},1}, P_{\mathrm{NBI},2}, \dot{\bar{n}}_\mathrm{i}, \bar{n}_\mathrm{i})$. By linearizing the system (9) with respect to the state and control around a nominal equilibrium point $(\boldsymbol{\omega}_\mathrm{eq},\boldsymbol{u}_\mathrm{eq})$ for $\boldsymbol{\delta} = 0$, we obtain the linear time-invariant model given by

$$\dot{\boldsymbol{\omega}} \approx \boldsymbol{F}\Big|_{\substack{\boldsymbol{\omega}_\mathrm{eq}\\ \boldsymbol{u}_\mathrm{eq}}} + \frac{\partial \boldsymbol{F}}{\partial \boldsymbol{\omega}}\Big|_{\substack{\boldsymbol{\omega}_\mathrm{eq}\\ \boldsymbol{u}_\mathrm{eq}}} (\boldsymbol{\omega}-\boldsymbol{\omega}_\mathrm{eq}) + \frac{\partial \boldsymbol{F}}{\partial \boldsymbol{u}^\mathrm{c}}\Big|_{\substack{\boldsymbol{\omega}_\mathrm{eq}\\ \boldsymbol{u}_\mathrm{eq}}} \tilde{\boldsymbol{u}} + \frac{\partial \boldsymbol{F}}{\partial \boldsymbol{u}^\mathrm{nc}}\Big|_{\substack{\boldsymbol{\omega}_\mathrm{eq}\\ \boldsymbol{u}_\mathrm{eq}}} \boldsymbol{d},$$

where $\tilde{\boldsymbol{u}}(t) = \boldsymbol{u}^\mathrm{c}(t) - \boldsymbol{u}^\mathrm{c}_\mathrm{eq}$, $\boldsymbol{d}(t) = \boldsymbol{u}^\mathrm{nc}(t) - \boldsymbol{u}^\mathrm{nc}_\mathrm{eq}$. After discretizing the linearized system with a semi-implicit scheme in time, we obtain the model,

$$\boldsymbol{\omega}_{k+1} = \boldsymbol{A}\boldsymbol{\omega}_k + \boldsymbol{B}\tilde{\boldsymbol{u}}_k + \boldsymbol{B}_d\boldsymbol{d}_k + \boldsymbol{f}_\omega, \tag{10}$$

where

$$\boldsymbol{A} = \left(\boldsymbol{I} - T_s \frac{\partial \boldsymbol{F}}{\partial \boldsymbol{\omega}}\Big|_{\substack{\boldsymbol{\omega}_\mathrm{eq}\\ \boldsymbol{u}_\mathrm{eq}}}\right)^{-1}, \quad \boldsymbol{B} = T_s\boldsymbol{A}\,\frac{\partial \boldsymbol{F}}{\partial \boldsymbol{u}^\mathrm{c}}\Big|_{\substack{\boldsymbol{\omega}_\mathrm{eq}\\ \boldsymbol{u}_\mathrm{eq}}},$$

$$\boldsymbol{B}_d = T_s\boldsymbol{A}\,\frac{\partial \boldsymbol{F}}{\partial \boldsymbol{u}^\mathrm{nc}}\Big|_{\substack{\boldsymbol{\omega}_\mathrm{eq}\\ \boldsymbol{u}_\mathrm{eq}}}, \quad \boldsymbol{f}_\omega = T_s\boldsymbol{A}\left(\boldsymbol{F}\Big|_{\substack{\boldsymbol{\omega}_\mathrm{eq}\\ \boldsymbol{u}_\mathrm{eq}\\ \boldsymbol{\delta}=0}} - \frac{\partial \boldsymbol{F}}{\partial \boldsymbol{\omega}}\Big|_{\substack{\boldsymbol{\omega}_\mathrm{eq}\\ \boldsymbol{u}_\mathrm{eq}}}\boldsymbol{\omega}_\mathrm{eq}\right),$$

and T_s is the time step. The affine term $\boldsymbol{f}_\omega$ arises due to the fact that we are writing the model in terms of the full state rather than the more common error state, i.e. the state relative to the equilibrium value, for reasons discussed in the next section.

C. Reference Tracking Problem via MPC

The reference tracking problem is formulated as a finite-horizon, optimal tracking control problem. At time k, consider the quadratic optimization problem

$$\begin{aligned}
\underset{\{\boldsymbol{\Delta}u_{k+t}\}_{t=0}^{H_u}}{\text{minimize}} \quad & J_k = \sum_{t=1}^{H_p} \|\boldsymbol{\omega}_{k+t} - \boldsymbol{r}_{k+t}\|_{\boldsymbol{Q}} + \sum_{t=0}^{H_u} \|\Delta\tilde{\boldsymbol{u}}_{k+t}\|_{\boldsymbol{R}} \\
\text{subject to} \quad & \boldsymbol{\omega}_{k+t+1} = \boldsymbol{A}\boldsymbol{\omega}_{k+t} + \boldsymbol{B}\tilde{\boldsymbol{u}}_{k+t} + \boldsymbol{B}_\mathrm{d}\boldsymbol{d}_{k+t} + \boldsymbol{f}_\omega \\
& \boldsymbol{\omega}_k = \boldsymbol{\omega}(k): \text{ initial condition} \\
& \Delta\tilde{\boldsymbol{u}}_k = \tilde{\boldsymbol{u}}_{k+1} - \tilde{\boldsymbol{u}}_k \\
& \tilde{\boldsymbol{u}}_{k-1} = \text{previously applied control} \\
& \boldsymbol{d}_{k+t} = \boldsymbol{d}_k \text{ for } t = 0,1,\ldots H_u \\
& \tilde{\boldsymbol{u}}_{k+t} \in \tilde{\mathcal{U}}_{k+t} \text{ for } t = 0,1,\ldots H_u
\end{aligned} \tag{11}$$

The cost function J_k includes an instantaneous cost on deviations of the measured outputs from the desired reference, $\boldsymbol{r}_k$, over the prediction horizon, H_p. Also, an instantaneous cost is applied to deviations in the control, $\Delta\tilde{\boldsymbol{u}} = \tilde{\boldsymbol{u}}_{k+1} - \tilde{\boldsymbol{u}}_k$, implying no cost for the control sequence to be away from the value associated with equilibrium operating point, $\boldsymbol{u}_\mathrm{eq}$, but there is a cost for fast rate changes. Predicting the state evolution in terms of the actual state with the use of the affine model (10) instead of a deviation term (error state) allows the controller to anticipate future reference changes. We allow the horizon associated with the control, H_u, to be less than the prediction horizon associated with the state, to reduce the complexity of the problem. We assume no further update in the control beyond the control horizon, i.e. $\tilde{\boldsymbol{u}}_{k+t} = \tilde{\boldsymbol{u}}_{k+t-1}$ for $t \ge H_u$ and we assume the uncontrolled actuators are constant ($\boldsymbol{d}_{k+t} = \boldsymbol{d}_k$). The term $\{\tilde{\boldsymbol{u}}_{k+t} \in \tilde{\mathcal{U}}_{k+t}\}_{t=0}^{H_u}$ describes linear constraints on the actuators to be described. The solution to this optimization problem, $\Delta\boldsymbol{U}^\star$, is a sequence of control decisions,

$$\Delta\tilde{\boldsymbol{U}}^\star = [\Delta\tilde{\boldsymbol{u}}_k^\star, \Delta\tilde{\boldsymbol{u}}_{k+1}^\star, \ldots, \Delta\tilde{\boldsymbol{u}}_{k+H_u}^\star].$$

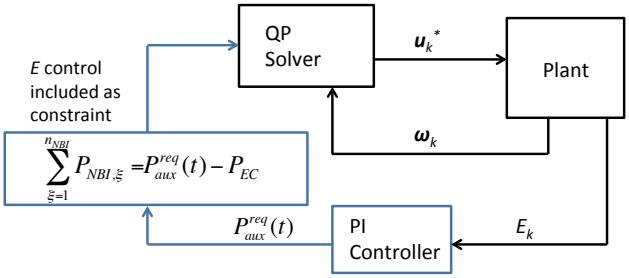

Fig. 3. Rotation profile MPC with total power constraint to satisfy desired plasma stored energy.

Of course, we cannot simply apply the resulting control sequence because the model used to predict the future states is not perfectly accurate. Therefore, the common practice is to apply the first step of the sequence, then sample the state again, and repeat the optimization procedure, which introduces feedback to the control.

For control design purposes the stored energy evolution is approximated by its linearized dynamics,

$$\frac{dE}{dt} = -\frac{E}{\tau_{\mathrm{E_{eq}}}} + P_{\mathrm{aux}}(t), \tag{12}$$

where the contributions of ohmic power and radiative power are dropped since they are relatively small compared to the auxiliary power, and $\tau_{\mathrm{E_{eq}}}$ is the global energy confinement time associated with the equilibrium point $(\boldsymbol{\omega}_{\mathrm{eq}}, \boldsymbol{u}_{\mathrm{eq}})$. The approximate energy dynamics (12) describe a linear first order system, therefore with a simple proportional-integral (PI) controller we can obtain acceptable closed loop performance. With the PI controller,

$$P_{\mathrm{aux}}^{\mathrm{req}}(t) = k_p(E^d(t) - E(t)) + k_i \int_0^t E^d(\tau) - E(\tau) d\tau, \tag{13}$$

we can obtain a request for total auxiliary input power, $P_{\mathrm{aux}}^{\mathrm{req}}(t)$, which can enter into the MPC problem as an equality constraint on the total auxiliary power. The combination of rotation profile MPC with energy control constraint is depicted in Fig. 3. The constraint on total auxiliary power can be written as

$$\sum_{\xi=1}^{n_{\mathrm{NBI}}} P_{\mathrm{NBI},\xi} + P_{\mathrm{EC}} = P_{\mathrm{aux}}^{\mathrm{req}}(t), \tag{14}$$

which represents a linear constraint on the control variables, therefore it can be incorporated without modification into problem (11) over the control horizon, H_u. In this manner we can obtain the desired plasma stored energy, and then allow the MPC controller to find the best combination of torque sources, NBI and NRMF, satisfying the total power constraint to match the desired rotation profile. The ECRH does not contribute any significant torque to the plasma, so it can essentially vary freely within its limits to satisfy the constraint (14).

D. Normalized Pressure Ratio (β_N) Limit

Deleterious MHD activity can be avoided by maintaing normalized β_N, β normalized to the plasma current, below $\beta_N^{\max}$. To help ensure stable plasma conditions during the discharge, we can predict changes to β_N over the prediction horizon and enforce a constraint in the total auxiliary power to maintain β_N below an acceptable limit. The normalized β can be expressed as $\beta_N = k_{\beta_N} \frac{E}{I_{\mathrm{p}}}$, where k_{β_N} is a constant depending on the plasma volume, plasma minor radius, and toroidal magnetic field.

At time k, we can take the current value of $\tau_{E,k}$ ($\tau_{E,k} \propto I_{\mathrm{p},k}^{0.93} \bar{n}_{\mathrm{e},k}^{0.41} P_{\mathrm{tot},k}^{-0.69}$) and current energy E_k, to estimate the forward evolution of β_N according to

$$\begin{aligned} E_{k+1} &= A_E E_k + B_E P_{\mathrm{aux},k}, \\ E_{k+2} &= A_E^2 E_k + A_E B_E P_{\mathrm{aux},k} + B_E P_{\mathrm{aux},k+1}, \\ E_{k+3} &= A_E^3 E_k + A_E^2 B_E P_{\mathrm{aux},k} + A_E B_E P_{\mathrm{aux},k+1} \\ &\qquad + B_E P_{\mathrm{aux},k+2}, \end{aligned} \tag{15}$$

$$\begin{aligned} E_{k+t} &= A_E^t E_k + \sum_{i=0}^{t-1} A_E^i B_E P_{\mathrm{aux},k+t-i}, \\ \beta_{N,k+t} &= k_{\beta_N} \frac{E_{k+t}}{I_{\mathrm{p},k+t}}, \end{aligned} \tag{16}$$

where $A_E = \left(1 + \frac{1}{\tau_{E,k}} T_s\right)^{-1}$ and $B_E = A_E T_s$. In this work I_{p} is assumed either constant or preprogrammed therefore the future I_{p} evolution is known and the constraint on β_N reduces to a maximum bound on requested auxiliary power. Combining (15) and (16), we can transform the β_N limit over the prediction horizon, $\beta_{N,k+t}|_{t=0,1,\ldots,H_p} \leq \beta_N^{\max}$ into a constraint on maximum auxiliary power input. In order to ensure the MPC problem remains feasible, potential conflicts between the β_N limit and the energy control constraint (14) are alleviated by softening the energy control constraint with a forgiveness parameter,

$$P_{\mathrm{aux}}^{\mathrm{req}}(t) - \epsilon_{\mathrm{E}} \leq \sum_{\xi=1}^{n_{\mathrm{NBI}}} P_{\mathrm{NBI},\xi} + P_{\mathrm{EC}} \leq P_{\mathrm{aux}}^{\mathrm{req}}(t) + \epsilon_{\mathrm{E}}, \tag{17}$$

where $\epsilon_E \geq 0$ represents a window on forgiveness of satisfying the energy control constraint. The forgiveness parameter is included as an optimization variable in the MPC problem (11) by replacing the optimization objective with

$$J_k + W_E \epsilon_E^2, \tag{18}$$

where W_E is introduced as a weight.

IV. Simulation Results

In this section, we present a simulation study of the controller's effectiveness. The target for Ω_ϕ is obtained from (1) with the input values and parameter profiles of DIII-D shot 147634, and the stored energy setpoint is simply set to 1 MJ, a typical value for H-mode plasmas. We use no feedforward control and allow the feedback controller alone to recover the target profile. The rotation evolution is modeled with equations (1)-(7).

The control-design problem consists of the selection of the diagonal elements of $\boldsymbol{Q}$ and $\boldsymbol{R}$, the prediction horizons H_p, and the control horizon H_u of the quadratic program (QP) (11). To solve the QP, we use an active set algorithm, and take advantage of warm-starting [16], [17]. Active set

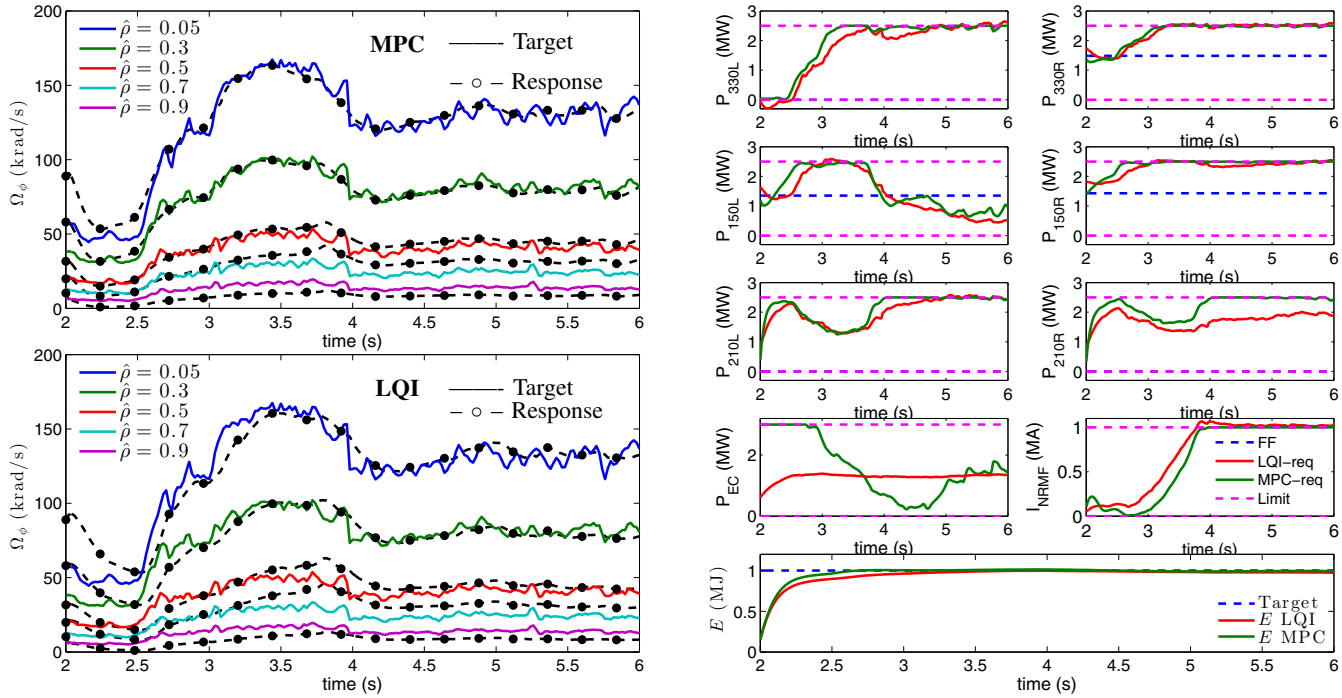

(a) Ω_ϕ: MPC (top) and LQI (bottom) (b) Inputs

Fig. 4. Feedback control simulation. (a) Ω_ϕ, where the solid line is the target and the achieved profile is marked by circles. (b) Input values and E, where the controller requested power is in green (MPC) and red (LQI), the blue dashed line marks the feedforward power, and the pink dashed line marks the actuators limits. The stored energy set point is marked by the blue dashed line.

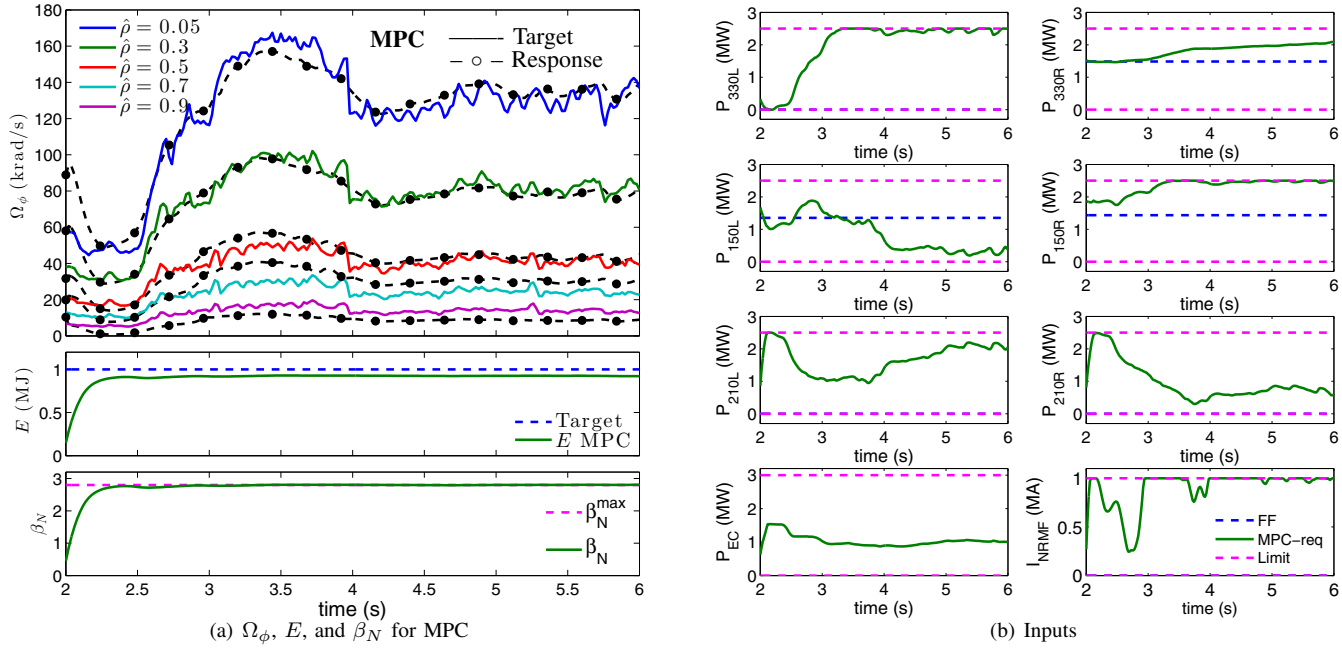

(a) Ω_ϕ, E, and β_N for MPC (b) Inputs

Fig. 5. Same simulation as in Fig. 4 with β_N limit imposed. The line and color configuration is also the same as in Fig. 4.

algorithms are essentially efficient methods for searching through the possible combinations of active inequality constraints, i.e. the inequality constraints that are satisfied as equalities at the optimal solution. Once the active set is known, the solution to a strictly convex quadratic program reduces to the solution of a linear system. Therefore most of the work of an active set algorithm is associated with determining the active set. Noting the active set does not change much from one control update to the next, we can use the active set from the previous MPC solution to *warm-start* the next MPC solution. We use a short horizon time of $H_p = 10$ and $H_u = 5$, which combined with warm-starting allows for an average computation time less than 3 ms.

In Fig. 4(b), we test the controller's tracking performance with feedback ON throughout the simulation. The target profile and simulated closed-loop profile response are plotted

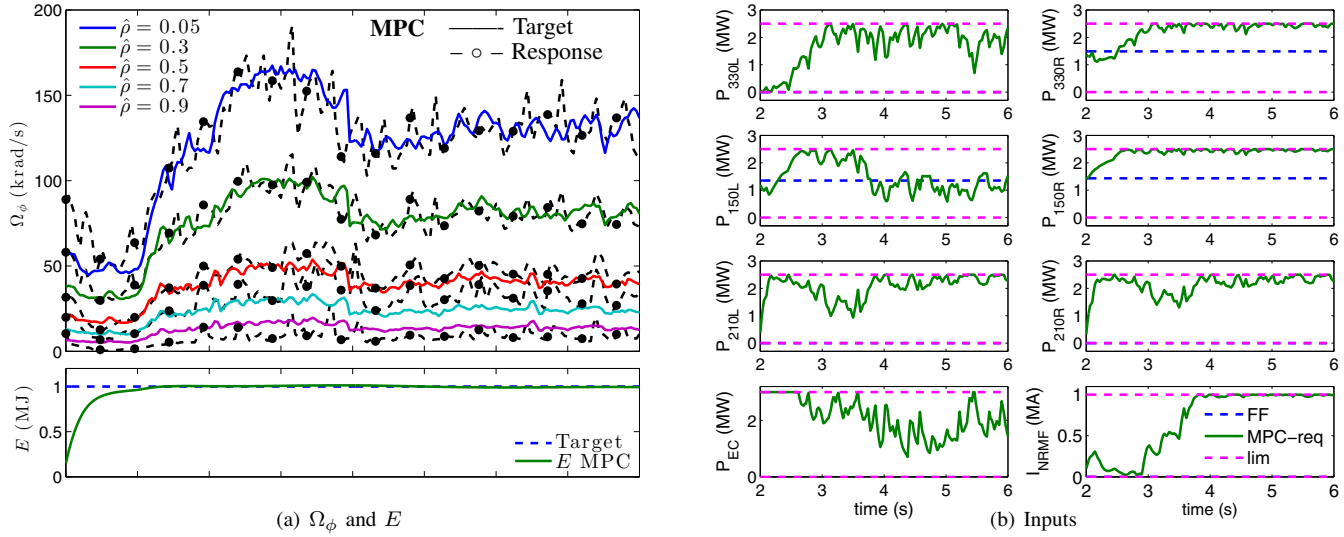

(a) Ω_ϕ and E (b) Inputs

Fig. 6. Same simulation as Fig. 4, except we allow χ_ϕ to vary randomly in the range shown in Fig. 2(b).

in 4(a), and the requested actuator powers[1] and plasma energy are plotted in Fig. 4(b). For comparison the results of both the MPC approach and the linear quadratic integral (LQI) approach of previous work [8] are both plotted in Fig. 4(a) under the same conditions (no β_N limit). The MPC profile controller performs well, enabling tight profile regulation while maintaining a nearly flat stored energy. At $t = 4$ s, the rotation profile target switches discretely to a lower target value. Note that the controller obtains the second, lower rotation target by increasing the counter-I_p NBI power (P_{210L} and P_{210R}) while reducing the co-I_p NBI power (P_{330L} and P_{150L}) to maintain the stored energy around the set point of 1 MW. The additional power from the ECRH is quite advantageous in maintaining the stored energy value and the NRMF provides some advantage over NBI in regulating the rotation at the plasma edge. The LQI controller performs similarly to the MPC; it lags the time changing target slightly due to the fact that the MPC anticipates future target changes. The main advantage of the MPC approach is the handling of actuator constraints, in particular the ability to impose the β_N limit as a variable total auxiliary power limit. In the second simulation, Fig. 5, we consider the MPC control approach again with the β_N limit imposed arbitrarily at $\beta_N^{\max} = 2.7$ for testing purposes. The target energy and rotation profile are met as closely possible while satisfying the β_N limit. In the third simulation, Fig. 6, the conditions are the same as the first except we allow for random perturbations in the value of χ_ϕ over the range depicted in Fig 2(b). This simulation provides a check of robustness against the anomalous properties of χ_ϕ.

V. Summary and Conclusions

We described a MPC reference tracking control approach for regulation of the toroidal rotation profile in the DIII-D tokamak that simultaneously maintains the desired plasma stored energy via a constraint on total auxiliary power. Additionally, the controller is designed to respect β_N limits to improve stability against deleterious MHD activity. The controller is formulated as a strictly convex QP and is solved using an active-set algorithm that exploits the consistency between active inequality constraints in subsequent control steps for fast computation speed. The simulations show promise of an effective controller for the combined control of rotation and energy using NBI, ECRH, and NRMF coils as actuators.

[1] P_{330L} and P_{330R} are co-current on-axis, P_{150L} and P_{150R} are co-current off-axis and P_{210L} and P_{210R} are counter-current on axis NBI.

References

[1] R. J. LaHaye, *Phys. Plasmas*, vol. 17, no. 056110, 2010.
[2] S. Sabbagh *et al.*, *Nucl. Fusion*, vol. 46, no. 23, pp. 635–644, 2006.
[3] F. L. Hinton and M. R. Rosenbluth, *Physics Letters A*, vol. 259, pp. 267–275, June 1999.
[4] R. C. Isler, *Phys. Plasmas*, vol. 17, no. 056110, 2010.
[5] W. Zhu *et al.*, *Physical Review Letters*, vol. 96, no. 225002, 2006.
[6] A. J. Cole *et al.*, *Physical Review Letters*, vol. 106, p. 225002, 2011.
[7] K. H. Finken *et al.*, *Phys. Rev. Lett.*, vol. 94, p. 015003, 2005.
[8] W. Wehner, J. Barton, and E. Schuster, "Toroidal Rotation Profile Control for the DIII-D Tokamak," in *Proceeding of the 2015 American Control Conference*, 2015.
[9] I. Goumiri *et al.*, "Modeling and control of plasma rotation for NSTX using neoclassical toroidal viscosity and neutral beam injection," *Nuclear Fusion*, vol. 56, no. 3, p. 036023, 2016.
[10] H. S. John, "Equations and associated definitions used in onetwo," p. 8, Nov 2005. [Online]. Available: https://fusion.gat.com/THEORY/onetwo/
[11] R. J. Goldston, "Basic physical processes of toroidal fusion plasmas," *Proc. Course and Workshop Varenna, 1985*, vol. 1, pp. 165–186, 1986.
[12] J. Barton *et al.*, "Physics-based Control-oriented Modeling of the Safety Factor Profile Dynamics in High Performance Tokamak Plasmas," *Proceeding of the 52nd IEEE International Conference on Decision and Control*, 2013.
[13] ITER Physics Basis, *Nuclear Fusion*, vol. 39, p. 2137, 1999.
[14] J. Wesson, *Tokamaks*. Oxford, UK: Clarendon Press, 1984.
[15] K. Kunisch and S. Volkwein, *Numerische Mathematik*, vol. 90, pp. 117–148, 2001.
[16] J. Nocedal and S. J. Wright, *Numerical Optimization 2nd edn.* Berlin: Springer, 2006.
[17] M. ApS, *The MOSEK optimization toolbox for MATLAB manual. Version 7.1 (Revision 28).*, 2015.